Head impacts in non-helmeted sports: Measuring and locating the impact force

Original Article

Institution of MECHANICAL ENGINEERS

Journal of SPORTS ENGINEERING AND TECHNOLOGY

Proc IMechE Part P:
J Sports Engineering and Technology
1–12

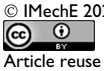
Article reuse guidelines:
sagepub.com/journals-permissions
DOI: 10.1177/17543371221130894
journals.sagepub.com/home/pip


Head impacts in non-helmeted sports: Measuring and locating the impact force

Jazim Sohail[1], Filipe Teixeira-Dias[1] and Susan Merriman[2]

Abstract

Mild traumatic brain injury within contact sports is a growing concern due to the serious risk of injury and concussion. Extensive research is being conducted looking into head kinematics during impacts in non-helmeted contact sports utilizing instrumented mouthguards, allowing researchers to record accelerations and velocities of the head during and after an impact. This does not, however, allow the location of the impact on the head, and its magnitude and orientation, to be determined. This research proposes and validates an algorithm using rigid body dynamics that approximates the impact force and determines its location and orientation from instrumented mouthguard kinematic data. Impact data captured from an experimental laboratory test using an instrumented mouthguard and five finite element simulations are used to validate the algorithm. The obtained results from both validation methods highlight the effectiveness of the proposed impact magnitude and location algorithm as impact locations were calculated within 12 mm of the impact center for all conducted tests. Additionally, components of force unit vectors (direction cosines) obtained from the algorithm were within ± 0.03, which equates to less than 11% of the components of applied force unit vectors, highlighting the accuracy of impact direction vector established from the algorithm. This algorithm has the potential to significantly aid researchers conducting field tests within non-helmeted sports by reducing the time required to analyze and determine head impact locations.

Keywords

Head impacts, non-helmeted sports, mTBI, impact measurement, concussion, instrumented mouthguard, rugby

Date received: 7 February 2022; accepted: 17 September 2022

Introduction

Non-helmeted contact sports are popular worldwide in a number of different forms, one of the most popular being Rugby Union which has a registered player base of 9.6 million and a fan base of 405 million worldwide.[1] The popularity within the sport arises due to it providing a combination of physical, mental, and skill challenges to the competitors that take part. The physical nature of rugby, however, does bring with it the potential for injuries, the most serious being mild Traumatic Brain Injury (mTBI).[2] mTBI is caused by a sudden blow or jolt to the head, a situation that occurs frequently within non-helmeted sports during games.[3,4] Head-to-head impacts are common within these sports, with head injuries accounting for 17% of injuries within Rugby Union.[5] Prien et al.[6] and Pfister et al.[7] conducted systematic reviews to analyze the number of concussive events seen within different sports at both professional and youth level. Their results showed concussion rates within rugby to be the highest, with 3 and 4.3 concussions recorded per 1000 Athletic Exposures (AE) within professional and youth level rugby match play, respectively.

These statistics highlight the importance in understanding the nature of impacts sustained by players in non-helmeted sports. Currently, understanding head kinematics during and after an impact, predominantly the linear and rotational acceleration of the head, is being extensively researched. Different methods have been proposed and used in the past to understand the kinematics of the human head during and after an impact, with video footage being the only source of data available at the early stages of this area of research.

[1]School of Engineering, The University of Edinburgh, Edinburgh, UK
[2]Force Impact Technologies, Inc., Gilbert, AZ, USA

Corresponding author:
Filipe Teixeira-Dias, Alexander Graham Bell building, School of Engineering, The University of Edinburgh, The King's Buildings, Edinburgh EH9 3FG, UK.
Email: f.teixeira-dias@ed.ac.uk

Figure 1. Instrumented mouthguard developed by Force Impact Technologies (FIT), used in this research.

McIntosh et al.[8] used video recordings of impacts to estimate the head impact velocity in two dimensions, allowing the estimation of the energy transfer to the head from an impact. This method, however, proved not to be an accurate way of understanding head kinematics due to the impact velocity being approximated as well as a number of parameters required for the calculations being estimated.

Wearable sensors housing accelerometers and gyroscopes were therefore utilized to provide head kinematic data to establish head impact trends within contact sports. For helmeted sports, head mounted sensors placed within helmets were utilized to quantify impacts. Researchers predominantly used the Head Impact Telemetry system which incorporated six single-axis linear accelerometers embedded in the padding of the helmet for studies in helmeted sports.[9–12] The accuracy of the kinematic data obtained from HIT and helmet mounted sensors was rigorously studied, with researchers establishing more than 15% error in resultant peak linear accelerations.[13–15] For non-helmeted sports, the skin patch was developed which is a skin mounted wireless sensor placed behind the ear of the player. It records and calculates key data when an impact occurs, such as linear acceleration and rotational velocity components of the head.[16] This technology was used extensively by King et al.,[17] Hecimovich et al.,[18] and Willmott et al.[19] within different levels of Australian Rules Football, from youth to sub-elite, and in amateur Rugby League. These authors were also able to establish head acceleration trends from impacts. However, studies have highlighted measurement error for peak resultant acceleration to be as high as 50% from the skin patch due to skin dynamics and lack of skull coupling.[13,20]

Further technological advancements saw the development of instrumented mouthguards,[21–25] such as the one shown in Figure 1, which house a sensor strip that captures kinematic data via a gyroscope and linear accelerometer. This is currently being used by different researchers as it allows more accurate data recording in comparison to the skin-mounted sensors. Wu et al.[26] established that mouthguards showed tighter skull couplings than skin mounted sensors, providing more accurate kinematic results. This technology has predominantly been used for research purposes within helmeted sports such as American football,[21–24] with only a small number of research projects focusing on non-helmeted sports. King et al.[27] conducted a preliminary study with an instrumented mouthguard, quantifying head impacts within amateur Rugby Union players. These authors were able to determine trends regarding the magnitudes of accelerations felt by players in different positions during a full season of matches.

The main aim of the research presented here is to propose and develop a method, algorithm and numerical tool that will allow researchers to analyze kinematic data from instrumented mouthguards. The data collected from the sensors is in the form of tri-axial acceleration and velocity components. The proposed method determines the location and orientation of the impact on the head, based in this recorded data. Little research has been conducted to propose a robust method to determine the impact locations from sensor data. In most reported cases, peak linear acceleration components are used to approximate the direction of impact and hence an impact location region (back, side, front).[28] Video footage is often utilized alongside to verify impact location regions, as PLA component based regions have shown inaccuracies.[23] In most cases, however, this is an extremely costly and time-consuming process. Crisco et al.[29] developed an algorithm that allows the location of an impact to be calculated. This algorithm is based on data collected from several single axis non-orthogonal accelerometers and was found to be an effective method for helmeted sports, where multiple accelerometers can be placed within the helmet. For instrumented mouthguards with a tri-axial linear accelerometer and gyroscope, Bartsch et al.[22] and Kuo et al.[23] proposed methodologies to approximate the location of the impact. Bartsch et al. utilized rigid body dynamics with assumptions, to simplify the problem to determine an approximated impact location whereas Kuo et al. utilized integrated linear and rotational position values to determine an impact region. The methodology proposed by Kuo et al., however, was only able to classify 37% of impacts to the correct impact region, highlighting the need for a methodology to improve upon the accuracy of impact location classification. The following section describes a proposed method, which builds on the work published by Bartsch et al.,[22] utilizing rigid body dynamics and a multi-degree of freedom (MDOF) lumped-mass system replicating the head and neck, to determine the orientation, magnitude, and location of an impact force from instrumented mouthguard data. Unlike the approaches by Bartsch et al. and Kuo et al., the following method aims to determine the impact location rather than a region of the head where the impact occurs. The accuracy of the impact location determined by the proposed method is established by

an author-defined metric as described in the following section. It is hypothesized, with the extensive data collection push expected in the near future, knowing where on the head the impact occurs will be very useful, as different areas of the same region (back/side/front) could be more or less susceptible to concussions, making the following methodology extremely useful in research in the battle against mTBI.

Methodology

The method proposed to determine the magnitude, orientation, and location of an impact based on mouthguard linear acceleration and rotational velocity components is based on rigid body dynamics. The main steps in the Impact Magnitude and Location Algorithm (IMLA) developed in this work can be summarized as:

1. Calculation of the components of the moment, from Euler's equations.
2. Estimation of the magnitude of the impact force with a multi-degree of freedom (MDOF) system. This is achieved with modal analysis to establish the mechanical response of the system in three linear directions.
3. Moment matching between Euler's and torque equations to determine the location of the impact.

Impact moment calculation

The moment experienced by the head because of the impact is first calculated using Euler's equations, where the Cartesian components of the moment vector $\boldsymbol{T}$ are

$$\boldsymbol{T} = \begin{Bmatrix} T_x \\ T_y \\ T_z \end{Bmatrix} = \begin{Bmatrix} I_{xx}\dot{\omega}_x - (I_{yy} - I_{zz})\omega_y\omega_z \\ I_{yy}\dot{\omega}_y - (I_{zz} - I_{xx})\omega_z\omega_x \\ I_{zz}\dot{\omega}_z - (I_{xx} - I_{yy})\omega_x\omega_y \end{Bmatrix} \quad (1)$$

where I_{ij}, with $i,j = x,y,z$ as shown in Figure 2, are the second moments of area about the head/C1 vertebrae joint, $\dot{\omega}_i$ are the rotational acceleration components of the head, and ω_i are the rotational velocity components of the head. The head/C1 vertebrae joint is used as the main rotation point to replicate realistic head motion. The parallel axis theorem is used to determine the second moment of area about the rotation point from the center of gravity.

Impact force magnitude

A three-dimensional mass-spring MDOF system is used to estimate the magnitude and direction of the impact force on the head. This 4-mass system replicates the human head and neck with the springs replicating the stiffness of the intervertebral joints. m_1 is the mass of the head and m_2, m_3, and m_4 are the masses of the cervical vertebrae pairs C1-C2, C3-C4, and C5-C6, respectively, as defined by Luo and Goldsmith.[30] The equations of motion of the system are

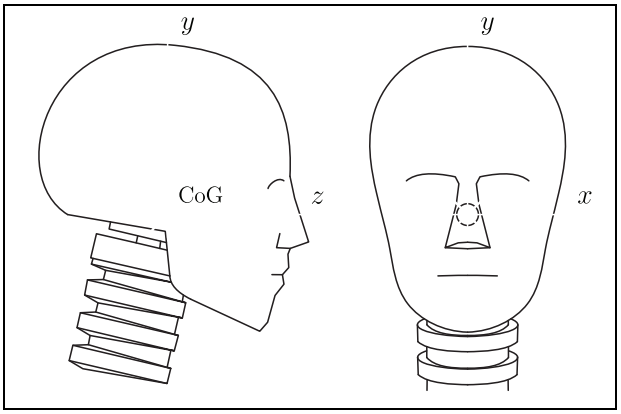

Figure 2. Global axis orientations. *xy* plane representing the coronal plane, *yz* plane representing the sagittal plane, and *xz* plane representing the transverse plane.

$$\mathbf{M}\ddot{\boldsymbol{x}} + \mathbf{K}\boldsymbol{x} = \boldsymbol{F} \quad (2)$$

where $\mathbf{M}$ and $\mathbf{K}$ are the inertia and stiffness matrices, and $\boldsymbol{F}$ is the vector of external forces acting on the system. Damping is not considered in the MDOF model as in the short impact times that are characteristic of head impacts in sports, there are no significant energy dissipation mechanisms and the response of the system is dominated by stiffness.

The stiffnesses of the intervertebral disks were determined by Luo and Goldsmith[30] using stiffness data previously reported by Deng and Goldsmith[31] and Panjabi,[32] considering that the stiffness of each individual joint is proportional to the cross-sectional area of the corresponding disk. These authors calculated a stiffness matrix for the C2/C3 joint and a proportionality factor for the remaining ones, allowing stiffness matrix calculations for any intervertebral joint. The (6×6) C2/C3 joint stiffness matrix supplied by Luo and Goldsmith[30] incorporates all six degrees of freedom, three linear and three rotational. As the MDOF system is a linear three-dimensional system, the stiffness matrix provided by Luo and Goldsmith[30] becomes

$$\mathbf{k} = \begin{bmatrix} 122 & 0 & 0 \\ 0 & 390 & 25 \\ 0 & 25 & 140 \end{bmatrix} \times 10^3 \quad [\mathrm{N/m}] \quad (3)$$

The individual springs $\mathbf{k}_i = \alpha\mathbf{k}$ ($i = 1, \ldots, 4$) are the (3×3) stiffness matrices for each joint, which replicate the head/C1, C2/C3, C4/C5, and C6/C7 intervertebral joints and α is the proportionality factor. The global stiffness matrix $\mathbf{K}$ then becomes

$$\mathbf{K} = \begin{bmatrix} \mathbf{k}_1 & -\mathbf{k}_1 & 0 & 0 \\ -\mathbf{k}_1 & \mathbf{k}_1 + \mathbf{k}_2 & -\mathbf{k}_2 & 0 \\ 0 & -\mathbf{k}_2 & \mathbf{k}_2 + \mathbf{k}_3 & -\mathbf{k}_3 \\ 0 & 0 & -\mathbf{k}_3 & \mathbf{k}_3 + \mathbf{k}_4 \end{bmatrix} \quad (4)$$

The global inertia matrix compiles the four individual mass matrices as

$$\mathbf{M} = \begin{bmatrix} \mathbf{m}_1 & 0 & 0 & 0 \\ 0 & \mathbf{m}_2 & 0 & 0 \\ 0 & 0 & \mathbf{m}_3 & 0 \\ 0 & 0 & 0 & \mathbf{m}_4 \end{bmatrix} \quad \text{with} \quad \mathbf{m}_i = \begin{bmatrix} m_i & 0 & 0 \\ 0 & m_i & 0 \\ 0 & 0 & m_i \end{bmatrix} \tag{5}$$

The inertia of the individual vertebrae couples and head are also taken from Lou and Goldsmith.[30]

The external force vector is the (12×1) matrix

$$\boldsymbol{F} = \begin{Bmatrix} F_x \\ F_y \\ F_z \\ 0 \\ \vdots \\ 0 \end{Bmatrix} \tag{6}$$

where F_x, F_y, and F_z are the unknowns of the problem. Note that, as the proposed method models head impacts, the only non-zero external forces are associated with $\mathbf{m}_1$.

Modal analysis is used to calculate the natural frequencies and mode shapes of the MDOF system, which are in turn used to determine the mechanical response of the system when a force is applied.[33] The equation of motion, equation (2), can then be rewritten as

$$\left(\mathbf{K}\mathbf{M}^{-1}\right)\boldsymbol{X}_i = w_i^2 \boldsymbol{X}_i \tag{7}$$

where $\boldsymbol{X}_i$ $(i = 1, \ldots, 12)$ are the system's mode shape vectors and w_i are the corresponding natural frequencies. The modal force vector $\boldsymbol{Q}$ can then be calculated as

$$\boldsymbol{Q} = \mathbf{X}^T \boldsymbol{F} \tag{8}$$

where $\mathbf{X}$ is the modal shape matrix. In order to determine the unknowns within the modal force, the following displacement equation is solved

$$\boldsymbol{x} = \mathbf{X}\boldsymbol{q} \tag{9}$$

where $\boldsymbol{x}$ is the displacement vector of the system, consisting linear displacements for all four masses, and $\boldsymbol{q}$ is the vector with components

$$q_i = \frac{1}{w_i}\left[\frac{Q_i}{w_i}(1 - \cos(w_i t))\right] \tag{10}$$

The linear acceleration components of the head are obtained directly from mouthguard data and then converted to linear acceleration components at the center of gravity (CoG) of the head with

$$\boldsymbol{a}_{CoG} = \boldsymbol{a}_M + \dot{\boldsymbol{\omega}} \times \boldsymbol{d} + \boldsymbol{\omega} \times \boldsymbol{\omega} \times \boldsymbol{d} \tag{11}$$

where $\boldsymbol{a}_M$ are the linear accelerations recorded at the mouthguard, $\dot{\boldsymbol{\omega}}$ and $\boldsymbol{\omega}$ are the rotational accelerations and velocities of the head, and $\boldsymbol{d}$ is the position vector of the CoG relative to the mouthguard. For the purpose of the IMLA, $\boldsymbol{d}$ was calculated by determining the distance from a selected node in the mouth of the Hybrid III Dummy head to the corresponding center of gravity.

Integrating $\boldsymbol{a}_{CoG}$ twice allows the displacement of the head to be calculated. By solving equation (9), the unknown components of the impact force within the modal force, equation (8), and unknown displacement components for the system can be calculated.

Impact location

The impact location was determined by matching the moments calculated with equation (1) and the torque equation

$$\boldsymbol{T}_t = \boldsymbol{r} \times \boldsymbol{F}_t \tag{12}$$

where $\boldsymbol{r}$ is the position vector from the axis of rotation, as defined in the impact moment calculation section, to a point on the surface of the skull. $\boldsymbol{F}_t$ is the force vector consisting of force components on the head as calculated from the MDOF system in equation (9).

For the purpose of the IMLA, the moments are calculated for coordinates on the surface of a head using equation (12). Coordinates can be established by utilizing nodes from a generic FE model or from MRI scans for specific players. Obtaining an MRI scan for every player within a team could be very impractical therefore the authors proposed that a generic FE model approach to be used with the IMLA. A three stage process is implemented to determine the location of the impact. Initially, the algorithm matches moment signs, eliminating nodes with position vector $\boldsymbol{r}$ that produce differentiating $\boldsymbol{T}_t$ component signs to $\boldsymbol{T}$. Secondly, moments values $\boldsymbol{T}_t$ not within $\boldsymbol{T} \pm 100\%$ are eliminated leaving a small cluster of nodes, providing an estimation of the impact location. For this algorithm a broad tolerance of $\pm 100\%$ established good results in identifying approximated impact regions. Finally, the tolerance is incrementally reduced until only one node is remaining, which is determined as the best fitting node (BFN) and the location of the impact on the surface of the head. For the purpose of this research, where coordinates were established from a Hybrid III Dummy model, The impact location calculated by the algorithm is deemed accurate and fit for purpose if the BFN matches the node of the impact center or is a neighboring node to the impact center. This equates to the calculated BFN being within 14 mm of the impact center, due to the mesh size of the Hybrid III Dummy head.

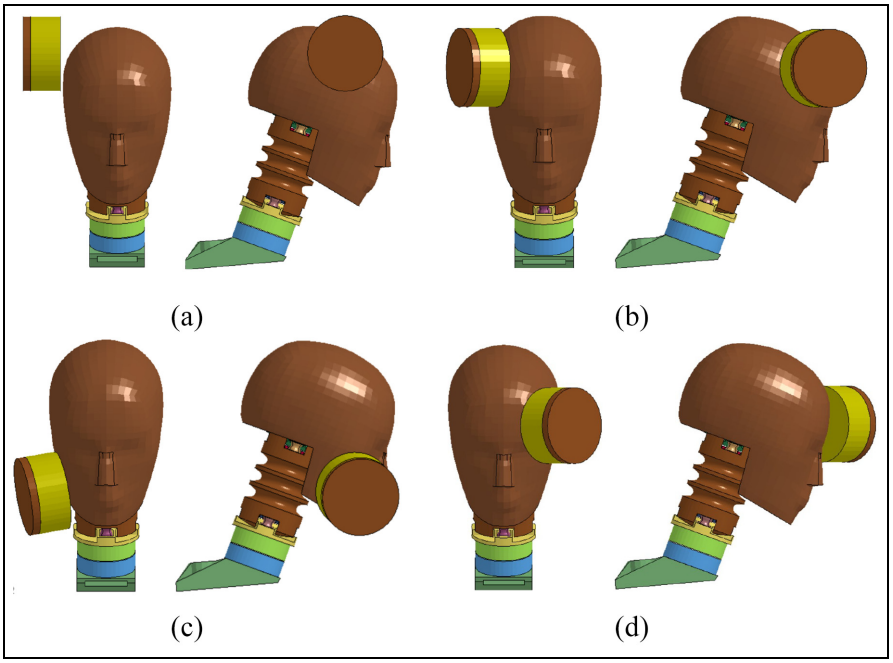

Figure 3. Finite Element (FE) simulation setups in LS-DYNA: (a) Test 1 and Test 4 replicating a side impact with impactor initial velocity in the *x* direction, (b) Test 2 replicating a left-front-side-upper impact with impactor initial velocity in the *x* and negative *z* direction, (c) Test 3 replicating a front-side-lower impact with impactor initial velocity in the *x*, *y*, and negative *z* direction, and (d) Test 5 replicating a right-front-side-upper impact with impactor initial velocity in the negative *x* and negative *z* direction.

Validation

The IMLA was validated by obtaining head impact kinematic data by two methods. The primary method used a head-neck finite element Hybrid III Dummy model simulating impacts on the dummy head. Impact simulations were conducted on different locations of the head, and the kinematic responses were used to validate the IMLA. Additionally, kinematic impact data was obtained in a laboratory test from an instrumented mouthguard similar to the one in Figure 1. The two methods complement each other to provide a validation of the proposed IMLA. The Hybrid III finite element (FE) simulations allow control over key impact parameters such as head dimensions, minimizing errors when testing the IMLA. Additionally, the simulations provide a method to test the developed algorithm against impacts of varying magnitudes and locations with ease. The observations from the experimental test ensure the IMLA is accurate and can be used to determine the location of live impacts when using instrumented mouthguards.

Numerical modeling

Five models were developed using a validated LS-DYNA Hybrid III Dummy head/neck model, consisting of 50,698 elements, 63,500 nodes with 176,682 degrees of freedom, created with hexahedral constant stress solid finite elements.[34,35]

Simulations were conducted to replicate impacts on different locations of the head as shown in Figure 3(a) to (d). Side, left-upper-side-frontal, right-upper-side-frontal, and lower-side-frontal locations were selected for impacts for the FE simulations with the laboratory test providing a frontal impact. Tests 1 and 4 were conducted from the same "Side" location with differing initial velocity components to test the IMLA with different impact levels at the same location. Boundary conditions were applied to the base of the shoulder piece to fix movement in all rotational and linear directions. Additionally, the simulation duration was set to 30 ms, with a data output time-step of 1 ms to replicate the instrumented mouthguard's operating frequency of 1000 Hz.

The material properties and initial conditions selected for the impactor were chosen to provide impact magnitudes and durations that closely reflect on-field impacts within rugby.[27] A cylindrical impactor with a diameter of 100 mm and a thickness of 40 mm was created with hexahedral solid reduced integration constant stress finite elements. The impactor consisted of 4329 nodes, 3680 elements with 12,987 degrees of freedom and a mesh size of 3.5 mm with Table 1 listing the impactor mass, density, and initial conditions for each test.

A hyper-elastic rubber constitutive law was used for the impactor (MAT 077 H on LS-DYNA) defined as

$$W(J_1, J_2, J) = \sum_{p,q=0}^{n} C_{pq}(J_1 - 3)^p (J_2 - 3)^q + W_h(J)$$

where W_h is the hydrostatic work and the required C_{pq} constants are $C_{10} = 1.07$, $C_{01} = 0.99$, $C_{11} = 0.99$, $C_{20} = 10$, $C_{02} = 0$, and $C_{30} = 10$ MPa. These constants

Table 1. Impactor setup and material properties.

	Test 1	Test 2	Test 3	Test 4	Test 5
Mass (kg)	12.5	12.5	12.5	12.5	12.5
Density (kg/m^3)	40,000	40,000	40,000	40,000	40,000
Initial $\boldsymbol{v}$ (m/s)					
x	2.5	1.5	1.5	1.0	−1.75
y	0.0	0.0	0.5	0.0	0.0
z	0.0	−1.5	−1.0	0.0	−1.75

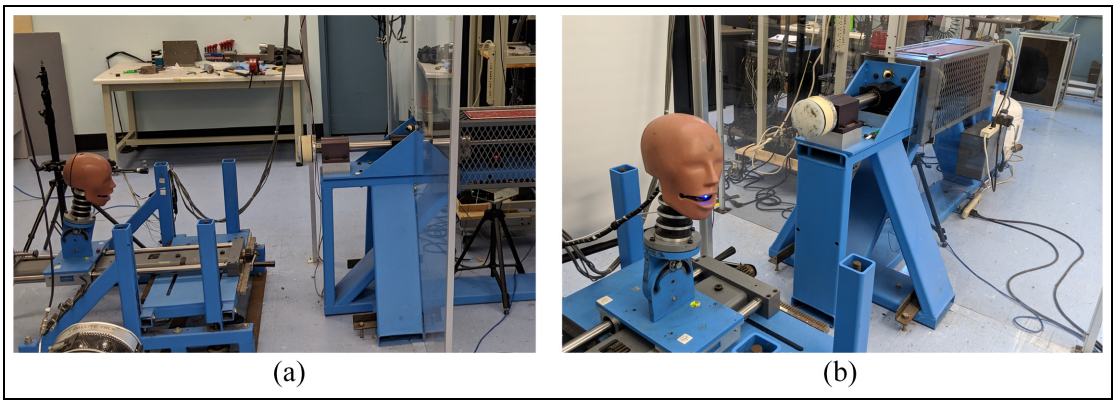

Figure 4. Biokinetics medium-velocity head impact laboratory simulator used to conduct the experimental lab tests: (a) showcasing the linear impactor, target table, head-form and (b) highlighting the position of the mouthguard within the head-form.

describe the strain energy functional, which is a function of the relative volume J and models hyper-elastic rubber behavior with $J_1 = I_1 I_3^{-1/3}$, $J_2 = I_2 I_3^{-2/3}$.[36]

Experimental tests

The experimental impact tests were done with a Biokinetics medium-velocity head impact simulator, shown in Figure 4,[37] instrumented with a mouthguard developed by Force Impact Technologies (FIT), similar to the one in Figure 1. A dental impression is taken of the dentition of the test head which is used to mold a custom fitted mouthguard that affixes securely to the dentition. The same process that is used to make a custom fitted mouthguard for a human athlete is used to mold the instrumented mouthguard for the test head. This mouthguard incorporates a sensor strip anterior to the upper incisors, similar to the one that is being implemented in instrumented mouthguards worldwide.[23–25] The sensors include a tri-axial linear accelerometer (ST H3LIS331DL) and a gyroscope (ST LSM6DS3H) providing linear acceleration (±200g @ 1000 Hz) and rotational velocity (±2000 dps @ 1666 Hz) data. The sensors are used in combination to implement an inertial measurement unit with data recorded over a 40 ms window. The test setup used to provide kinematic data to test the IMLA was a right-frontal impact with a 14 kg impactor at 5 m/s. The instrumented mouthguard was positioned over the upper dentition of the test head, replicating the location of an instrumented mouthguard during live impacts.

Results

Kinematic data

Kinematic data obtained from the experimental test measurements and finite element simulations are shown in Figure 5 and Table 2. The linear acceleration data in Figure 5 is collected from the instrumented mouthguard that shows the impact occurring at around 6 ms with a noticeable peak linear acceleration of −8g, 77g, and −46g in the x, y, and z directions, respectively, at approximately 11 ms. The rotational velocity calculated from the lab test shows a constant increase after the impact in the negative x and positive z directions, as expected from a right-frontal impact. Rotational velocity values reached −15 and 14 rad/s in the x and z directions, respectively. From the obtained kinematic data, the impact duration of the lab test was found to be in the 8–12 ms range. The linear acceleration in the y direction approaches 0 at around 1.4 ms whereas in the z direction this happens at around 1.8 ms.

The kinematic response of the FE models shows similarities to the laboratory test with regards to the duration and magnitude of the impacts. The impactor material properties were selected to ensure the FE simulations that utilized a validated Hybrid III Dummy head model, provided acceleration magnitudes that replicated head impacts within non-helmeted sports. The impact durations for all FE simulations are within a 8–12 ms range as seen in Table 2. Impact durations were established by analyzing the contact data between the head and impactor, as well as the kinematic output

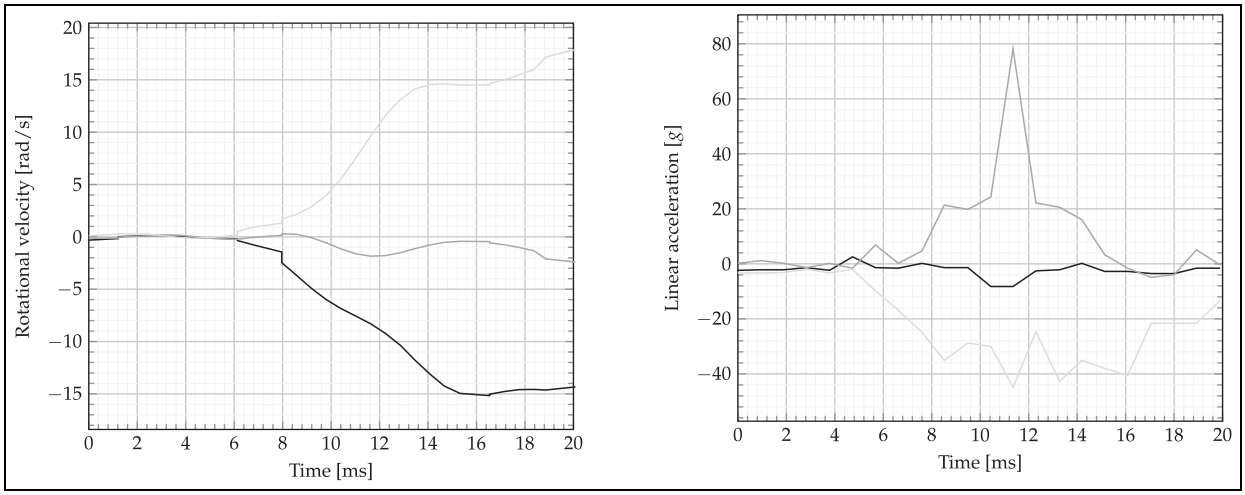

Figure 5. Kinematic response of the head during the lab test collected via FIT instrumented mouthguard in the *x* (▬), *y* (▬), and *z* (▬) directions: rotational velocity (left) and linear acceleration (right).

Table 2. Kinematic results from LS-DYNA simulations.

	PLA (**g**)				$\boldsymbol{\omega}$ at PLA (**rads**$^{-1}$)				Duration (**ms**)
	a_x	a_y	a_z	$\boldsymbol{a}$	ω_x	ω_y	ω_z	$\boldsymbol{\omega}$	
Test 1	100	−10	−5	100.6	−1	−0.2	−13	13	9
Test 2	50	−2	−14	52	0.5	13	−4	13.6	8
Test 3	45	24	−9	51.8	0.8	5.2	9.6	10.9	10.6
Test 4	29	−2.8	−1.6	29.2	−0.38	−0.7	−5.5	5.6	11.8
Test 5	−48	10	−40	63.3	−0.3	−10	4	10.8	8

as described for the lab test. Additionally, Peak linear acceleration (PLA) as seen in Table 2, were 100.6*g*, 52*g*, 51.8*g*, 29.2*g*, and 63.3*g* for Tests 1–5 respectively. Finally, the angular velocity obtained with the FE model were of similar magnitude to the lab test. Table 2 highlights the rotational velocity ($\boldsymbol{\omega}$) components for all tests during the PLA phase of the impacts.

Impact location and direction

The IMLA was used for all validation simulations to establish the location of the impact. Figures 6 and 7 show the direct output from the IMLA, which generates all the analyzed coordinates on the surface of the head and highlights the BFN as the calculated location of the impacts. The experimental test was a right frontal impact, replicated by the algorithm, as shown in Figure 6(e). Additionally, for the Hybrid Dummy III finite element simulations, the BFNs calculated by the IMLA for all impacts correlated to nodes that were struck by the impactor in the simulations.This can be seen when comparing Figure 3 with the IMLA output in Figures 6 and 7. As the impactor strikes more than one node, the distance from the BFN to the impact epicenter, which was defined as the initial point of contact between the impactor and the Hybrid III head, was calculated to quantify the accuracy of the impact location. The BFN for Tests 4 and 5 replicated the same node as the epicenter of the impact however, for Tests 1–3, the calculated BFN was found to be a neighboring node with the impact epicenter being a distance of 10.8, 9.9, and 11.6 mm away respectively.

Furthermore, Figure 7 highlights the impact location process for Test 3, as described in the methodology section. The initial stage of the process matches moment directions which eliminates the majority of the nodes as shown in Figure 7(a). Further nodes are eliminated by the addition of tolerances while matching moments and ensuring the impact vector can physically target the node, leaving a cluster of nodes in the cheek/jaw region, as seen in Figure 7(b). At this stage, a good approximation of the impact location can be determined, however the BFN can be established by reducing tolerances for each direction as highlighted in Figure 7(c).

Moreover, components of $\boldsymbol{T}$ established from equation (1) for the peak acceleration phase of each impact, components of $\boldsymbol{T_t}$ from equation (12) for the BFN and the tolerance ($\boldsymbol{\delta}$) components required for the algorithm to establish the BFN for all conducted tests can be seen in Table 3. The $\boldsymbol{\delta}$ components are established relative to components of $\boldsymbol{T}$ using

$$\boldsymbol{\delta} = 100\left(\frac{\boldsymbol{T} - \boldsymbol{T_t}}{\boldsymbol{T}}\right) \tag{13}$$

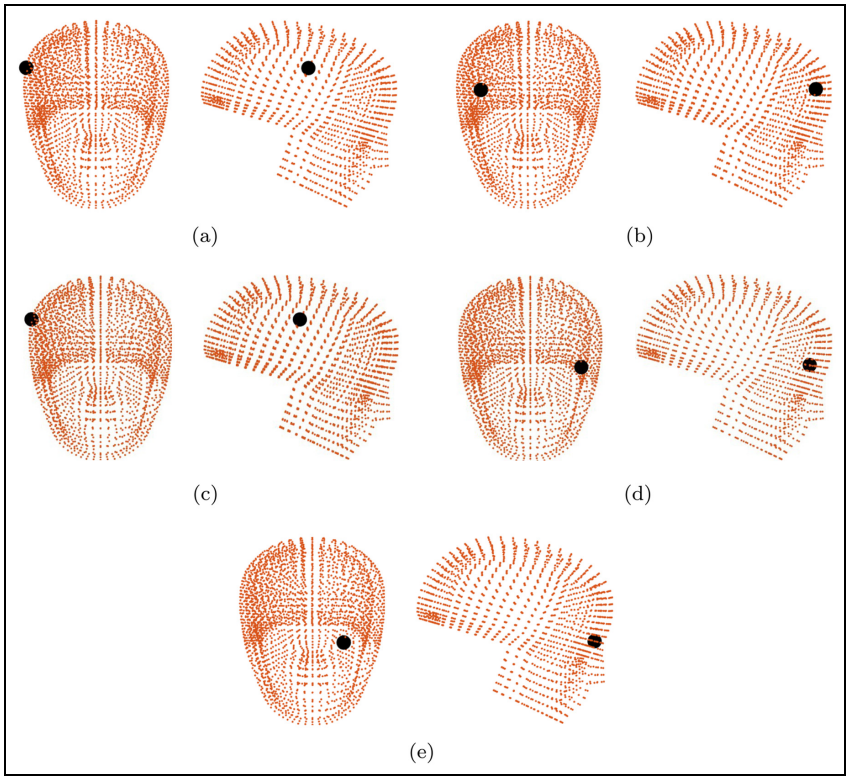

Figure 6. Impact location, highlighted in black, on the *xy* and *yz* planes for: (a) Test 1, (b) Test 2, (c) Test 4, (d) Test 5, and (e) experimental test as determined by the IMLA.

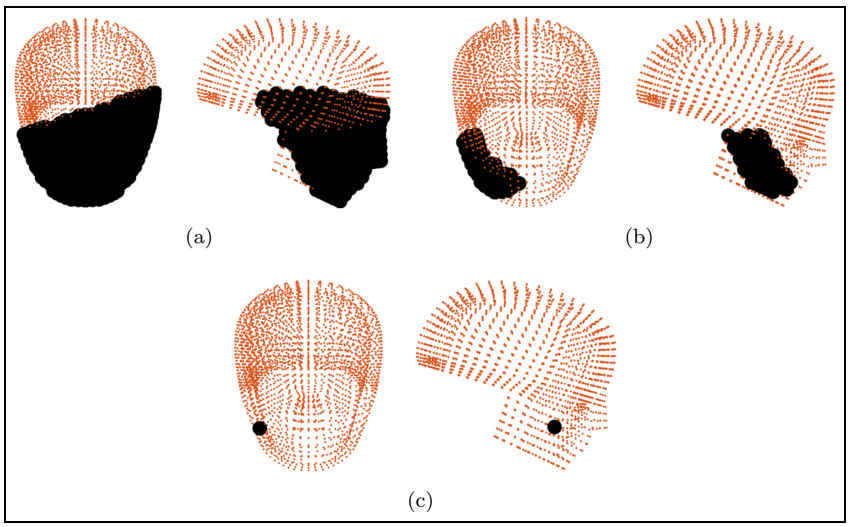

Figure 7. Impact location process for Test 3 on the *xy* and *yz* planes: (a) matching $\boldsymbol{T}$ and $\boldsymbol{T}_t$ signs, (b) matching $\boldsymbol{T} \pm 100\%$ and $\boldsymbol{T}_t$ values, and (c) reducing tolerances to find the BFN.

Table 3. Moment values as calculated from Euler's and torque equations.

	$\boldsymbol{T}$ (Nm)			$\boldsymbol{T}_t$ (Nm)			δ (%)		
	T_x	T_y	T_z	T_{tx}	T_{ty}	T_{tz}	δ_x	δ_y	δ_z
Test 1	−3.1	29.8	−83.3	−3.8	26.9	−82.5	22.5	9.7	1.0
Test 2	−4.0	81.0	−30.0	−3.9	81.8	−29.9	0.3	1.0	1.0
Test 3	−4.6	41.9	22.7	−7.0	30.0	23.3	52.2	28.4	2.6
Test 4	−1.0	8.4	−22.8	−0.8	7.7	−23.7	20.0	8.3	3.9
Test 5	−19.9	−51.6	23.9	−24.0	−46.1	17.0	20.6	10.7	28.9
Lab	−14.5	−2.5	17.3	−17.2	−2.0	4.5	18.6	20.0	74.0

Table 4. Magnitude of the impact force as measured by the MDOF model ($\boldsymbol{F_t}$) and comparison between the orientations of the applied force (direction cosines) as obtained by the numerical model ($\hat{\boldsymbol{F}}_s$) and the IMLA ($\hat{\boldsymbol{F}}_t$). The relative difference between the two approaches is also listed (Δ).

Test	Component	$\boldsymbol{F_t}$[N]	$\hat{\boldsymbol{F}}_s$	$\hat{\boldsymbol{F}}_t$	Δ (%)
Test 1	x	1230	0.99	0.99	0.13
	y	−150	−0.12	−0.12	2.52
	z	−102	−0.07	−0.08	6.94
Test 2	x	900	0.92	0.93	0.75
	y	−81	−0.09	−0.08	8.13
	z	−333	−0.37	−0.35	4.14
Test 3	x	550	0.91	0.91	0.23
	y	230	−0.36	−0.38	4.67
	z	−110	−0.21	−0.18	10.68
Test 4	x	400	0.99	0.99	0.60
	y	−46	−0.1	−0.11	6.86
	z	−27	−0.06	−0.06	4.76
Test 5	x	−834	−0.75	−0.75	0.43
	y	177	−0.15	−0.16	5.26
	z	−710	−0.66	−0.64	2.42
Lab	x	−118	–	−0.16	–
	y	250	–	0.35	–
	z	−660	–	−0.92	–

Additionally, Table 4 lists the approximated force, $\boldsymbol{F_t}$, established from the MDOF and the corresponding unit vector ($\hat{\boldsymbol{F}}_t$), as well as the unit vector of the applied force in the simulation ($\hat{\boldsymbol{F}}_s$) to determine the accuracy of the impact directions as calculated by the IMLA. As seen in Table 4, the difference between components of $\hat{\boldsymbol{F}}_s$ and $\hat{\boldsymbol{F}}_t$ are within ± 0.03 with the $\%\Delta$ relative to $\hat{\boldsymbol{F}}_s$ being less that 11% for all conducted tests, highlighting the accuracy at which the IMLA calculates impact direction.

Discussion

The proposed algorithm utilizes rigid body motion dynamics to establish impact locations, building upon the work of Bartsch et al.[22] However, unlike the assumption that the head rotates about the CoG made by Bartsch et al., the IMLA establishes rotations about the head/C1 joint and uses an additional MDOF system to replicate the kinematics of the head and neck to determine the impact direction, rather than assuming it is a free body. Furthermore, the IMLA determines position vectors and inertias from a Hybrid III Dummy model, incorporating the non-spherical shape of the human head, as opposed to using a simpler spherical geometry. Finally, the moment matching technique allows nodes to be eliminated till the BFN is found, rather than determining the position vector, as stated by Bartsch et al. Rather than approximating an impact region, this technique provides the ability to pinpoint the impact location to within 14 mm of the impact center, as highlighted in the Results section.

Tables 3 and 4 highlight the numerical output from the algorithm with regards to Eulers moments, Torque moments, approximated force magnitude, and impact direction. The approximated force components calculated by the MDOF is underestimated, however the impact direction vector is unaffected, with components of $\hat{\boldsymbol{F}}_t$ being within ± 0.03 of the components of $\hat{\boldsymbol{F}}_s$, as can be seen in Table 4, due to the components of the force all being underestimated by the same fraction. Despite the underestimated nature of the approximated force magnitude, the components of $\boldsymbol{T}_t$ listed in Table 3 for the BFN closely reflect the components of $\boldsymbol{T}$ established by equation (1). This observation is potentially due to the head and neck acting as a two pivot point system as described by Van Drunen,[38] resulting in only a fraction of the total impact force rotating the head about the head/C1 joint. The approximated nature of the impact force magnitude causing rotations about the head/C1 joint is hypothesized as the primary reason for the difference between the components of $\boldsymbol{T}$ and $\boldsymbol{T}_t$ listed in Table 3 for all impacts.

Moreover, the difference seen in Table 3 for the experimental test was larger than that of the FE simulations with δ_z being as high as 74%. One potential reason for this could be due to the FIT instrumented mouthguard gyroscope and linear accelerometers operating at different frequencies, as stated in the validation section. For the purpose of the IMLA, rotational velocity components were established for the timestamp with the lowest delta to the linear acceleration components. This results in rotational velocity components utilized in equation (1), and linear acceleration components in equation (11) being for differing time stamps which in turn means $\boldsymbol{T}$ and $\boldsymbol{T}_t$ values are obtained for differing timestamps. Some leading mouthguards in use currently house an accelerometer and gyroscope that operate at the same frequency. However, like the FIT mouthguard, some mouthguards house sensors that operate at differing frequencies, and therefore will induce small errors as kinematic data required for the IMLA will be obtained for differing timestamps.[39]

Furthermore, the experimental test replicated a live impact to validate the IMLA with variables that would be unknown to researchers utilizing instrumented mouthguards. Player heads vary in size and shape and it is not possible to accurately measure head dimensions when analyzing impacts which in turn will incur errors within variables such as $\boldsymbol{r}$ and $\boldsymbol{d}$ that require accurate distances. For the experimental test, the head shape utilized differed from the Hybrid III however, the coordinates required to establish $\boldsymbol{r}$ in equation (12) were obtained from the nodes on the surface of the Hybrid III Dummy FE model and the head/C1 rotation point of the Hybrid III. Additionally, $\boldsymbol{d}$ was also determined from the Hybrid III which will incur errors within the algorithm. A detailed sensitivity analysis was conducted to establish how sensitive a_{CoG} and $\boldsymbol{T}_t$ are to changes in $\boldsymbol{d}$ and $\boldsymbol{r}$. The observations listed in Table 5 show that a change in $\boldsymbol{d}$ by 1% results in a change of 0.15%, 0.11%, and 0.07% in a_{CoGx}, a_{CoGy}, a_{CoGz}, respectively, meaning that inaccuracies within $\boldsymbol{d}$ do not

Table 5. Sensitivity analysis of components of a_{CoG} to changes in d.

%Δ d	%Δ a_{CoGx}	%Δ a_{CoGy}	%Δ a_{CoGz}
−30	−4.58	3.20	−2.15
−20	−3.03	2.13	−1.43
−10	−1.51	1.06	−0.72
10	1.51	−1.08	0.72
20	3.04	−2.15	1.45
30	4.55	−3.22	2.17

Table 6. Sensitivity analysis of components of T_t to changes in r.

%Δ r	%Δ T_{tx}	%Δ T_{ty}	%Δ T_{tz}
−30	−30.04	−30.41	−30.13
−20	−20.03	−20.41	−20.17
−10	−10.02	−10.41	−10.17
10	10.02	10.41	10.13
20	20.03	20.41	20.17
30	30.05	30.41	30.17

alter the IMLA's output significantly. Inaccuracies within d are expected as the position vector from the CoG to the mouthguard would be estimated for live impacts as it is not possible to calculate the distance accurately in humans. Changes in r, however, were found to be proportional to changes in components of T_t, highlighting the sensitive nature of components of T_t to changes in r as can be seen in Table 6. The sensitive nature of r could result in the IMLA returning an impact location out with the 14 mm tolerance, if the shape of the head differs significantly from that of the FE head model. The test conducted in the laboratory, however, highlighted that head shape differing to the FE model still provided correct impact locations, with higher tolerances required to establish the BFN.

Moreover, inertia values used in equation (1) are established from the Hybrid III, which will result in small errors due to the shape of the Hybrid III Dummy differing from the head-form used in the experimental test.

The algorithm is, nonetheless, efficient in determining the location of the impact by eliminating nodes until only one remains, meaning the moments difference between T and T_t due to the discrepancies stated above does not hinder the algorithm's ability to provide an accurate impact location. However, further testing is required with live impact data collected from instrumented mouthguards to establish if the supplied methodology is able to provide accurate impact locations for varying scenarios seen within non-helmeted contact sports.

Conclusion

An algorithm to determine the impact magnitude and location of an impact on the head was developed to aid ongoing research regarding head impacts in non-helmeted contact sport. The algorithm utilizes a combination of rigid body dynamics and a multi degree of freedom (MDOF) system, and is validated with kinematic data from Hybrid III Dummy FE simulations and laboratory testing with an instrumented mouthguard. The five FE simulations and the laboratory test replicated impacts of varying magnitudes and locations to test the performance of the proposed algorithm (IMLA). The output from the algorithm correctly determines the impact locations for the simulations as the best fitting node (BFN) calculated by the IMLA is within 14 mm of the impact center for all conducted tests, meeting the criteria for an accurate impact location. Additionally, the mean percentage difference in moments values established from Euler's equation and the torque equation for FE Tests 1–5 were calculated to be 11%, 0.7%, 27.7%, 10.7%, and 20%. As expected, however, the mean percentage difference for the laboratory test was 37.7% and therefore higher tolerances than the FE simulations were required to determine impact locations due to the uncertainty in head dimensions. Further testing with live on field impacts is required to test the methodology however the IMLA has the potential to significantly aid researchers conducting field tests within non-helmeted sports with instrumented mouthguards by reducing the time required to analyze kinematic data and determine head impact locations.

Acknowledgements

For the purpose of open access, the authors have applied a Creative Commons Attribution (CC BY) license to any Author Accepted Manuscript version arising from this submission.

Declaration of conflicting interests

The author(s) declared no potential conflicts of interest with respect to the research, authorship, and/or publication of this article.

Funding

The author(s) disclosed receipt of the following financial support for the research, authorship, and/or publication of this article: The authors acknowledge the support given to this project by the Engineering and Physical Sciences Research Council (EPSRC) [grant: EP/R513209/1].

ORCID iD

Filipe Teixeira-Dias https://orcid.org/0000-0001-5854-5466

References

1. Rugby W. Global reach of Rugby 2019. Technical report, World Rugby, 2019.

2. Kerr HA, Curtis C, Micheli LJ, et al. Collegiate rugby union injury patterns in New England: a prospective cohort study. *Br J Sports Med* 2008; 42(7): 595–603.
3. Stemper BD and Pintar FA. Biomechanics of concussion. *Concussion* 2014; 28: 14–27.
4. VanItallie TB. Traumatic brain injury (TBI) in collision sports: possible mechanisms of transformation into chronic traumatic encephalopathy (CTE). *Metab Clin Exp* 2019; 100: 153943.
5. Tucker R. Head injury events in rugby union: description of high risk tackle events. *Br J Sports Med* 2017; 51(4): 398.
6. Prien A, Grafe A, Rossler R, et al. Epidemiology of head injuries focusing on concussions in team contact sports: a systematic review. *Sports Med* 2018; 48(4): 953–969.
7. Pfister T, Pfister K, Hagel B, et al. The incidence of concussion in youth sports: a systematic review and metaanalysis. *Br J Sports Med* 2016; 50(5): 292–297.
8. McIntosh AS, McCrory P and Comerford J. The dynamics of concussive head impacts in rugby and australian rules football. *Med Sci Sports Exerc* 2000; 32(12): 1980–1984.
9. Guskiewicz KM, Mihalik JP, Shankar V, et al. Measurement of head impacts in collegiate football players: relationship between head impact biomechanics and acute clinical outcome after concussion. *Neurosurgery* 2007; 61(6): 1244–1253.
10. Brolinson PG, Manoogian S, McNeely D, et al. Analysis of linear head accelerations from collegiate football impacts. *Curr Sports Med Rep* 2006; 5(1): 23–28.
11. Funk JR, Rowson S, Daniel RW, et al. Validation of concussion risk curves for collegiate football players derived from HITS data. *Ann Biomed Eng* 2012; 40(1): 79–89.
12. Schnebel B, Gwin JT, Anderson S, et al. In vivo study of head impacts in football: a comparison of National Collegiate Athletic Association Division I versus high school impacts. *Neurosurgery* 2007; 60(3): 490–496.
13. O'Connor KL, Rowson S, Duma SM, et al. Head-impact–measurement devices: a systematic review. *J Athl Train* 2017; 52(3): 206–227.
14. Allison MA, Kang YS, Bolte JH, et al. Validation of a helmet-based system to measure head impact biomechanics in ice hockey. *Med Sci Sports Exerc* 2014; 46(1): 115–123.
15. Jadischke R, Viano DC, Dau N, et al. On the accuracy of the Head Impact Telemetry (HIT) system used in football helmets. *J Biomech* 2013; 46(13): 2310–2315.
16. Tiernan S, Byrne G and O'Sullivan DM. Evaluation of skin-mounted sensor for head impact measurement. *Proc IMechE, Part H: J Engineering in Medicine* 2019; 233(7): 735–744.
17. King DA, Hume P, Gissane C, et al. Measurement of head impacts in a senior amateur rugby league team with an instrumented patch: exploratory analysis. *ARC J Res Sports Med* 2017; 2(1): 9–20.
18. Hecimovich M, King D, Dempsey A, et al. Youth australian footballers experience similar impact forces to the head as junior-and senior-league players: a prospective study of kinematic measurements. *J Sports Sci Med* 2018; 17(4): 547.
19. Willmott C, McIntosh AS, Howard T, et al. SCAT3 changes from baseline and associations with X2 patch measured head acceleration in amateur Australian football players. *J Sci Med Sport* 2018; 21(5): 442–446.
20. Wu LC, Laksari K, Kuo C, et al. Bandwidth and sample rate requirements for wearable head impact sensors. *J Biomech* 2016; 49(13): 2918–2924.
21. Camarillo DB, Shull PB, Mattson J, et al. An instrumented mouthguard for measuring linear and angular head impact kinematics in American football. *Ann Biomed Eng* 2013; 41(9): 1939–1949.
22. Bartsch A, Samorezov S, Benzel E, et al. Validation of an "intelligent mouthguard" single event head impact dosimeter. Technical report, SAE Technical Paper, 2014.
23. Kuo C, Wu L, Loza J, et al. Comparison of video-based and sensor-based head impact exposure. *PLoS One* 2018; 13(6): e0199238.
24. Hernandez F, Wu LC, Yip MC, et al. Six degree-offreedom measurements of human mild traumatic brain injury. *Ann Biomed Eng* 2015; 43(8): 1918–1934.
25. Rich AM, Filben TM, Miller LE, et al. Development, validation and pilot field deployment of a custom mouthpiece for head impact measurement. *Ann Biomed Eng* 2019; 47(10): 2109–2121.
26. Wu LC, Nangia V, Bui K, et al. In vivo evaluation of wearable head impact sensors. *Ann Biomed Eng* 2016; 44(4): 1234–1245
27. King D, Hume PA, Brughelli M, et al. Instrumented mouthguard acceleration analyses for head impacts in amateur rugby union players over a season of matches. *Am J Med* 2015; 43(3): 614–624.
28. Crisco JJ, Fiore R, Beckwith JG, et al. Frequency and location of head impact exposures in individual collegiate football players. *J Athl Train* 2010; 45(6): 549–559.
29. Crisco JJ, Chu JJ and Greenwald RM. An algorithm for estimating acceleration magnitude and impact location using multiple nonorthogonal single-axis accelerometers. *J Biomech Eng* 2004; 126(6): 849–854.
30. Luo Z and Goldsmith W. Reaction of a human head/neck/torso system to shock. *J Biomech* 1991; 24(7): 499–510.
31. Deng YC and Goldsmith W. Response of a human head/neck/upper-torso replica to dynamic loading—II. Analytical/numerical model. *J Biomech* 1987; 20(5): 487–497.
32. Panjabi MM. Three-dimensional mathematical model of the human spine structure. *J Biomech* 1973; 6(6): 671–680.
33. Rao SS. *Mechanical vibrations*. Upper Saddle River, NJ: Prentice Hall, 2011.
34. Kan CD, Marzougui D and Bedewi NE. Development of a 50th percentile Hybrid III dummy model. In: *Proceedings of the fourth European LS-DYNA users conference*, Ulm, Germany, 22 May 2003, pp.22–23.
35. Kang S and Xiao P. Comparison of Hybrid III rigid body dummy models. In: *10th international LSDYNA users conference*, 2008.
36. LSTC. LS-DYNA Keyword User's Manual Volume II Material Models LS-Dyna R7.1, 2014.
37. Siegmund GP, Guskiewicz KM, Marshall SW, et al. A headform for testing helmet and mouthguard sensors that measure head impact severity in football players. *Ann Biomed Eng* 2014; 42(9): 1834–1845.
38. Van Drunen P. *Identification of a two pivot human neck model using linear anterior-posterior perturbations*. Master's Thesis, Delft University of Technology, The Netherlands, 2009.
39. Liu Y, Domel AG, Yousefsani SA, et al. Validation and comparison of instrumented mouthguards for measuring

head kinematics and assessing brain deformation in football impacts. *Ann Biomed Eng* 2020; 48(11): 2580–2598.

Appendix

Notation

$\boldsymbol{a}$	Linear acceleration vector (numerical)
$\boldsymbol{a_{Cog}}$	Linear acceleration vector at centre of gravity
$\boldsymbol{a_M}$	Linear acceleration vector at mouthguard
$\boldsymbol{d}$	Distance vector from mouth to centre of gravity
$\boldsymbol{k}$	Local stiffness matrix
$\mathbf{m}$	Local inertia matrix
$\boldsymbol{r}$	Distance vector from centre of gravity to surface of head
t	Time
$\boldsymbol{v}$	Velocity vector
w	Natural frequency
$\ddot{\boldsymbol{x}}$	Acceleration vector
$\boldsymbol{x}$	Displacement vector
C_{pq}	Hyper-elastic rubber constants
$\boldsymbol{F}$	External force vector
$\hat{\boldsymbol{F}}_{\boldsymbol{s}}$	Applied force unit vector (numerical)
$\boldsymbol{F}_t$	Approximated force vector
$\hat{\boldsymbol{F}}_{\boldsymbol{t}}$	Approximated force unit vector
J	Relative volume
$\mathbf{K}$	Global stiffness matrix
$\mathbf{M}$	Global inertia matrix
$\boldsymbol{Q}$	Modal force vector
$\boldsymbol{T}$	Euler's moment vector
$\boldsymbol{T_t}$	Moment vector (from torque equation)
W	Work from hyper-elastic constitutive law
W_h	Hydrostatic work
$\mathbf{X}$	Modal shape matrix
$\boldsymbol{\delta}$	Tolerance vector
$\dot{\boldsymbol{\omega}}$	Rotational acceleration vector
$\boldsymbol{\omega}$	Rotational velocity vector